Structural Eng./Earthquake Eng., JSCE, Vol. 15, No. 2, 201s—213s, 1998 October
(J. Struct. Mech. Earthquake Eng., JSCE, No. 605/ I —45)

A THREE-DIMENSIONAL NONLINEAR SEISMIC ANALYSIS OF FRAMES CONSIDERING PANEL ZONE DEFORMATIONS

Xiao-Song LI[1] and Yoshiaki GOTO[2]

[1] Mem. of JSCE, Dr. Eng., Research Associate, Dept. of Civil Eng., Nagoya Institute of Technology
[2] Mem. of JSCE, Dr. Eng., Prof., Dept. of Civil Eng., Nagoya Institute of Technology
(Gokiso-cho, Showa-ku, Nagoya 466-8555, Japan)

In the conventional studies on the seismic behavior of bridge piers, it is common to use an in-plane modeling where the real behavior of frames subjected to the three-dimensional seismic loading is ignored. Herein, we present a three-dimensional nonlinear dynamic analysis for frames, where the panel zone deformation is also considered. In this analysis, geometrical nonlinearity is precisely taken into account by using the co-rotational method, whilst the member plastification is analyzed by the plastic-zone method. With the numerical method, the three-dimensional seismic behavior is examined for bridge piers of single post-type and portal frame-type in which effect of panel-zone deformation is also discussed.

Key Words: *nonlinear dynamic analysis, seismic design, space frame, panel zone.*

1. INTRODUCTION

In the conventional seismic design and analysis of steel bridge piers, it is common to adopt in-plane modeling. However, the validity of the in-plane modeling is not necessarily confirmed, because the three-dimensional seismic behavior of steel bridge piers has not been studied enough. Furthermore, the analysis model for the portal-frame type bridge piers mostly ignores the panel zone deformation and adopts the centerline-to-centerline geometry. This implies that neither the deformation nor the size of beam-to-column connections is considered in the analysis. However, the results of experiments have shown that beam-to-column joint deformation (panel zone) can significantly affect the overall behavior of frames [1), 2), 3)].

Some papers focused on the effect of panel zone deformation on the behavior of entire frames. Kato et al [4), 5)] presented a finite element model that took into account the shear deformation of panel zone and compared the results with those obtained for the frames with rigid beam-to-column connections or centerline-to-centerline geometry. They showed that in the elastic range, the solution based on the centerline-to-centerline modeling gave a good approximation to the exact solution considering the panel zone shear deformation. In the plastic range, however, the difference becomes remarkable. Lui and Chen [6)] showed a finite element model for panel zones that consists of one web element and two flange elements in order to consider both shear and bending deformations. Based on their research, Liew and Chen [7)] showed two criteria for the design of beam-column panel zones. Leger et al[8)] used a joint element to consider the rigid kinematic motion, elastic shear, and bending deformations of beam-column panel zone regions. A parametric analysis was carried out on the seismic response of in-plane frames. Without introducing an additional degree of freedom, Tsai and Popov[9)] presented an approximate method which considered the drift of elastic frames due to panel zone deformation. In their method, however, the axial force and P-delta effect were not included. They also confirmed that the centerline modeling of frames well approximates the behavior of frames with the shear panel zone deformation in the elastic range. More recently, Miki et al [10), 11)] employed a shear model to represent the panel zone deformation and examined its effect on the seismic behavior of portal frame-type bridge piers. All the above studies, however, were restricted to the in-plane behavior.

The purpose of this paper is to present a three-dimensional nonlinear dynamic analysis method for frames, where both geometric and material nonlinearities are considered. Furthermore, the shear deformation of panel zones is taken into account.

With the proposed numerical method, the three-dimensional seismic behavior is examined for the bridge piers of single-post type and the portal-frame type. In this investigation, the effect of panel zone deformation is also discussed.

2. NUMERICAL METHOD FOR GEOMETRIC AND MATERIAL NONLINEAR ANALYSIS OF SPACE FRAMES

(1) General

We have shown a rigorous numerical method for the geometrically nonlinear analysis of elastic space frames[12] where the finite rotations in three-dimensional space was precisely taken into account by the co-rotational technique. Here we extend it to the elasto-plastic dynamic analysis. To consider the material nonlinearity, a mixed strain-hardening bi-linear model is employed based on the von Mises yield criterion. In addition to the Saint-Venant's torsional deformation, the transverse shear deformation is taken into account in view of the fact that the stocky beams and columns are often used for bridge piers. To represent the transverse shear deformation, we adopt the Timoshenko beam model. In the finite element approximation for a beam element, displacement functions are chosen such that both normal and shear strains become constant along the length of an element in order to avoid the numerical integration over the element length and enhance the computational efficiency.

The basic assumptions adopted in the present analysis are (1) strains are small although rotations and displacements are large; (2) plane normal to the beam axis before deformation remains plane but not normal to the beam axis after deformation; (3) cross section is thin-walled doubly symmetric for elasto-plastic analysis.

(2) Geometric nonlinearity

In the present method, the geometric nonlinearity is considered by the co-rotational method. The details of the co-rotational method have been shown by Goto et al [12]. Therefore, we here briefly explain the method.

Two coordinate systems shown in **Fig.1** are used to derive the element stiffness equation. One is the fixed rectangular Cartesian coordinate system (x,y,z) with base vectors (g_x,g_y,g_z) defined in terms of the initial configuration of a beam element. The other is the orthogonal co-rotational coordinate system $(\bar{x},\bar{y},\bar{z})$ with base vectors $(\bar{i}_x,\bar{i}_y,\bar{i}_z)$ and the origin located at one end of the element. This

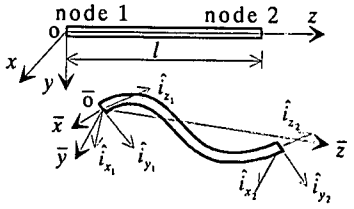

Fig.1 Coordinate systems

coordinate system moves with the rigid body rotation of the beam element. The directions of $(\bar{x},\bar{y},\bar{z})$ are defined to coincide with the averaged directions of the two sets of the deformed base vectors $(\hat{g}_{x_i},\hat{g}_{y_i},\hat{g}_{z_i})$ at nodes 1 and 2. The rotations of the deformed element are expressed by the unit vectors $(\hat{i}_{x_i},\hat{i}_{y_i},\hat{i}_{z_i})$ obtained by normalizing $(\hat{g}_{x_i},\hat{g}_{y_i},\hat{g}_{z_i})$.

The relations of the base vectors between the two coordinate systems are expressed by using the transformation matrices $[R_i]$ and $[R_G]$ as follows

$$\begin{Bmatrix}\hat{i}_{x_i}\\ \hat{i}_{y_i}\\ \hat{i}_{z_i}\end{Bmatrix}=[R_i]\begin{Bmatrix}g_x\\ g_y\\ g_z\end{Bmatrix};\quad \begin{Bmatrix}\bar{i}_x\\ \bar{i}_y\\ \bar{i}_z\end{Bmatrix}=[R_G]\begin{Bmatrix}g_x\\ g_y\\ g_z\end{Bmatrix} \qquad (1a,b)$$

where $[R_i]$ and $[R_G]$ are expressed by Euler angles $(\phi_i,\ \theta_i,\psi_i)$ and averaged Euler angles $(\bar{\phi},\ \bar{\theta},\bar{\psi})$ of two nodes, respectively. Eq.(1b) implies that the directions of the co-rotational coordinates $(\bar{x},\bar{y},\bar{z})$ are coincident with those of averaged Euler angles of $(\hat{i}_{x_1},\hat{i}_{y_1},\hat{i}_{z_1})$ and $(\hat{i}_{x_2},\hat{i}_{y_2},\hat{i}_{z_2})$.

Then, with some manipulations, the relation of incremental displacements between the member coordinates (x,y,z) and the co-rotational coordinates $(\bar{x},\bar{y},\bar{z})$ is obtained as

$$\{\Delta\bar{d}\}=[R]\{\Delta d\} \qquad (2)$$

where $[R]$ is a 6×12 transformation matrix.

Based on the virtual work principle[12], the following relation holds

$$\{f\}^T\{\Delta d\}=\{\bar{f}\}^T\{\Delta\bar{d}\} \qquad (3)$$

Substituting Eq.(2) into Eq.(3) and taking the increment lead to

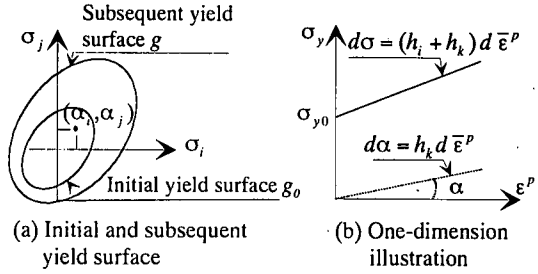

(a) Initial and subsequent yield surface (b) One-dimension illustration

Fig.2 mixed strain-hardening model

$$\{\Delta f\} = \left([R]^T [\Delta \bar{k}] [R] + \frac{\partial [R]^T}{\partial d} \{\bar{f}\} \right) \{\Delta d\} = [\Delta k] \{\Delta d\} \tag{4}$$

where $[\Delta \bar{k}]$ is the stiffness matrix of a Timoshenko beam element defined in terms of the co-rotational coordinate system. This stiffness matrix is obtained based on the small displacement beam theory and will be explained later. $[\Delta k]$ is the tangent stiffness matrix defined in terms of the member coordinate system (x, y, z). It should be noted here that the symmetry of $[\Delta k]$ is recovered only at equilibrium in state as pointed out by Simo and Vu-Quoc [13].

The transformation of stiffness equations from the member coordinates to the global coordinates fixed in space is the same as that of the usual finite element method.

(3) Material nonlinearity

Elasto-plastic stress-strain relation used in the present paper is based on von Mises yield criterion, associated flow rule and a mixed strain-hardening (kinematic and isotropic) rule as shown in **Fig.2**. For a thin-walled member, the yield function can be expressed as

$$g(\sigma, \alpha) = \sqrt{(\sigma - \alpha_1)^2 + 3(\tau - \alpha_2)^2} \tag{5}$$

where α_i is a back stress; σ is a normal stress due to axial and bending deformations; τ is a shear stress due to Saint-Venant's torsional deformation and transverse shear deformation.

The incremental elasto-plastic stress-strain relation is expressed as follows

$$\{d\sigma_i\} = [\mathbf{D}_{ep}] \{d\varepsilon_i\}; \; E^p = E^t / (1 - E^t / E) \tag{6a, b}$$

where

$$[\mathbf{D}_{ep}] = \begin{bmatrix} E & 0 \\ 0 & G \end{bmatrix} - \frac{1}{E^p g^2 + (\sigma - \alpha_1)^2 E + 9(\tau - \alpha_2)^2 G} \begin{bmatrix} (\sigma - \alpha_1)^2 E^2 & 3EG(\sigma - \alpha_1)(\tau - \alpha_2) \\ Sym. & 9G^2 (\tau - \alpha_2)^2 \end{bmatrix} \tag{6c}$$

where E and G are Young's elastic modulus and shear modulus, respectively; E^p and E^t are hardening modulus and elasto-plastic tangent modulus, respectively. Here, a bi-linear strain-hardening model is employed. Based on the mixed strain-hardening rule, we have

$$dg = h_i\, d\bar{\varepsilon}^p \; ; \quad \frac{\partial g}{\partial \sigma_i} d\alpha_i = h_k\, d\bar{\varepsilon}^p \tag{7a, b}$$

where h_i and h_k are isotropic and kinematic hardening moduli, respectively. E^p is equal to the sum of h_i and h_k. $\bar{\varepsilon}^p$ is the equivalent plastic strain. The increment of the back stress $d\alpha_i$ is determined based on the Ziegler's kinematic hardening rule as

$$\{d\alpha_i\} = \frac{h_k \left(\frac{\partial g}{\partial \sigma_i} d\sigma_i \right)}{(h_i + h_k) g} \{\sigma_i - \alpha_i\} \tag{8}$$

The change of the stress state from elasticity to plasticity or from plasticity to elasticity will lead to the change of stress-strain relation. Furthermore, loading will cause stresses to fall outside of the yield surface. Therefore, a return mapping method has to be employed to draw the stresses back to the yield surface. The various methods for return mapping have been presented [14] [15]. Herein, a 'Backward Euler Return' method summarized by Crisfield [16] is employed and extended to the mixed strain-hardening model.

(4) Finite element approximation

In the present study, a Timoshenko beam model based on the small displacement theory is used [17] in the co-rotational coordinate system $(\bar{x}, \bar{y}, \bar{z})$. This is because the displacement components defined in the co-rotational coordinates can be considered small from the assumption (1) stated in **Section 2 (1)**.

According to the assumption (2), the rotations of the transverse plane around the co-rotational

coordinate $\bar{x}$ and $\bar{y}$ axes can be expressed as

$$\bar{\theta}_x = \bar{v}_{,z} - \gamma^b_{yz} \; ; \quad \bar{\theta}_y = \bar{u}_{,z} - \gamma^b_{xz} \qquad (9a, b)$$

where $(\bullet)_{,z}$ denotes a partial differential with respect to $\bar{z}$. γ^b is the shear strain due to the transverse shear deformation. The axial displacement and rotations are approximated by linear functions, while the transverse displacements are approximated by quadratic polynomials as

$$\bar{w} = a_0 + a_1\bar{z}\,;\ \bar{u} = b_0 + b_1\bar{z} + b_2\bar{z}^2\,;\ \bar{v} = c_0 + c_1\bar{z} + c_2\bar{z}^2\,;$$
$$\bar{\theta}_z = d_0 + d_1\bar{z}\,;\ -\bar{\theta}_x = e_0 + e_1\bar{z}\,;\ \bar{\theta}_y = f_0 + f_1\bar{z} \qquad (10a\sim f)$$

With the assumption that transverse shear strain is constant along the element length, the constants in the displacement functions can be determined and expressed by the nodal displacements as follows:

$$\begin{aligned}
\bar{w} &= N_1\bar{w}_1 + N_2\bar{w}_2\,;\\
\bar{u} &= N_1\bar{u}_1 + N_3\bar{\theta}_{y_1} + N_2\bar{u}_2 - N_3\bar{\theta}_{y_2}\,;\\
\bar{v} &= N_1\bar{v}_1 - N_3\bar{\theta}_{x_1} + N_2\bar{v}_2 + N_3\bar{\theta}_{x_2}\,;\\
\bar{\theta}_z &= N_1\bar{\theta}_{z_1} + N_2\bar{\theta}_{z_2}\,;\\
\bar{\theta}_x &= -N_1\bar{\theta}_{x_1} - N_2\bar{\theta}_{x_2}\,;\\
\bar{\theta}_y &= N_1\bar{\theta}_{y_1} + N_2\bar{\theta}_{y_2}
\end{aligned} \qquad (11a\sim f)$$

where

$$N_1 = 1 - \bar{z}/l\,;\ N_2 = \bar{z}/l\,;\ N_3 = \bar{z}/2(1-\bar{z}/l) \qquad (12a\sim c)$$

Thus, the normal strain and shear strain of a finite element can be given as

$$\begin{aligned}
\varepsilon_z &= \bar{w}_{,z} - \bar{x}\,\bar{\theta}_{y,z} - \bar{y}\,\bar{\theta}_{x,z} = [N_\varepsilon]\{\bar{d}\}\,;\\
\gamma_{xz} &= \bar{u}_{,z} - \bar{\theta}_y + \Theta\bar{\theta}_{z,z} = [N_{\gamma x}]\{\bar{d}\}\,;\\
\gamma_{yz} &= \bar{v}_{,z} - \bar{\theta}_x + \Theta\bar{\theta}_{z,z} = [N_{\gamma y}]\{\bar{d}\}
\end{aligned} \qquad (13a\sim c)$$

where both $[N_\varepsilon]$ and $[N_{\gamma x(y)}]$ are independent of axial coordinate $\bar{z}$; that is, ε and γ are constants over the element length; $\Theta = 2n$ for open cross section; $\Theta = 2n - \oint h_n^* ds \,/\, \oint 1/t\, ds$ for closed cross section[18]. n is the normal distance from the centerline of the thin wall and t is the thickness of the wall. h_n^* is the distance from the shear center to the centerline.

Assuming the absence of distributed loads, the stiffness equation for a beam element in the co-rotational coordinates $(\bar{x}, \bar{y}, \bar{z})$ can be derived, based on the principle of virtual work as

$$\int_v \delta\{\Delta\varepsilon\}^T \{\Delta\sigma\} dv - \delta\{\Delta\bar{d}\}^T \{\Delta\bar{f}^e\} = 0 \qquad (14)$$

where $\{\Delta\bar{f}^e\}$ are the incremental nodal loads. By substituting Eqs.(6a), (13) into Eq.(14) and noting that the transverse displacement components at node 1 are zero and the rotational displacement components at nodes 1 and 2 have the same quantities but opposite sign, an elasto-plastic tangent stiffness equation expressed in terms of the co-rotational coordinates is obtained. Since both normal and shear strains are constants over the element length because of the adopted displacement functions, the numerical integration can be avoided in Eq.(14). The cross sectional area of the beam element is divided into elementary areas in order to take into account the plastification, following the customary procedures of the plastic zone method. The internal nodal forces are evaluated by the method shown in Reference 19) and 20). An incremental stiffness equation so obtained is expressed as

$$\{\Delta\bar{f}\} = [\Delta\bar{k}]\{\Delta\bar{d}\} \qquad (15)$$

Finally, substitution of Eq.(15) into Eq.(4) yields the elasto-plastic tangent stiffness matrix $[\Delta k]$ expressed in terms of the member coordinate system fixed in space.

(5) Equations of motion

In the present analysis, the mass of the body is assumed to be preserved so that the mass matrix can be evaluated prior to the time integration by using the initial configuration at time 0 as a reference state (Bathe et al [21]). Similarly, a mass proportional damping matrix is introduced. Thus, by incorporating Eq.(4), the incremental equations of motion for the member coordinates are expressed as

$$[M]\{\Delta\ddot{d}\} + [C]\{\Delta\dot{d}\} + [\Delta k]\{\Delta d\} = \{\Delta P_e\} \qquad (16)$$

where $[M]$ is the lumped mass matrix; $[C] = \alpha[M]$ is the damping matrix. In the present paper, $\alpha = 0$ is assumed in the following calculation.

To solve the overall incremental equations of motion, we employ the Newmark's β method ($\beta = 0.25$) combined with the Newton-Raphson iterative procedures. This iterative procedure is

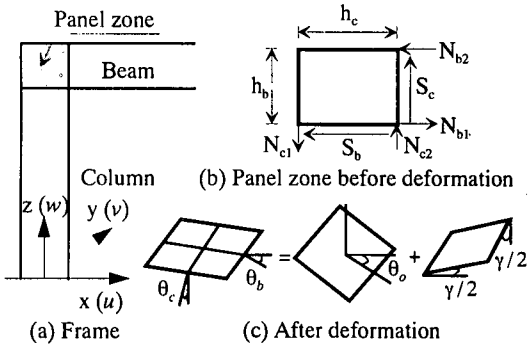

Fig.3 Deformation of panel zone

continued until the equilibrium or the convergence criterion $\|\psi\| \le \beta\|\mathbf{P}\|$ is satisfied, where ψ is the unbalanced force vector between internal nodal force vector and external nodal force vector **P**, β is a prescribed value of error tolerance and is set to 10^{-3} throughout this paper.

3. ANALYSIS OF BEAM-TO-COLUMN PANEL ZONE

(1) Modeling of panel zone

Portal frame-type bridge piers generally have quite large member dimensions so that the deformations of beam-to-column connection may not be neglected. As pointed out by some researchers, the deformations, mainly due to the shear deformation of panel zone, may have a significant effect on frame lateral stiffness and strength. To consider this effect, various models have been shown and compared with experimental results. Here, a three-dimensional modeling of panel zone is developed and incorporated in the nonlinear frame analysis explained in **Section 2**. In the present model, only in-plane shear deformation of panel zone is considered [11], while the out-plane deformation is ignored; that is, panel zone rotates as a rigid body around x-axis.

The rotations of the cross sections of a beam and a column that are connected to a panel zone are no longer equal to each other due to shear deformation of the panel zone as illustrated in **Fig.3**. In terms of the co-rotational coordinate system, the geometric relations between these rotations can be expressed as follows:

$$\begin{aligned} &\bar{\theta}_{cy} = \bar{\theta}_{oy} - \gamma/2\ ; \quad \bar{\theta}_{by} = \bar{\theta}_{oy} + \gamma/2\ ; \\ &\bar{\theta}_{oy} = (\bar{\theta}_{cy} + \bar{\theta}_{by})/2\ ; \quad \gamma = \bar{\theta}_{by} - \bar{\theta}_{cy} \end{aligned} \tag{17a~d}$$

where $\bar{\theta}_{oy}$ is the rotation of panel zone center; $\bar{\theta}_{cy}$ and $\bar{\theta}_{by}$ are the rotations of the ends of the column and beam, respectively, connected to the outer surfaces. γ is the shear strain of panel zone, which is assumed to be uniformly distributed. Furthermore, by considering the out-of-plane rigid body motion of the panel zone, the total displacement relations between the panel zone center and the ends of columns and beams can be obtained as follows:

a . Panel zone center to column end relation:

$$\begin{aligned} \{\Delta\bar{d}_c\} &= \{\Delta\bar{u}_c, \Delta\bar{v}_c, \Delta\bar{w}_c, \Delta\bar{\theta}_{cx}, \Delta\bar{\theta}_{cy}, \Delta\bar{\theta}_{cz}\}^T \\ &= \begin{bmatrix} 1 & 0 & 0 & 0 & -h_b/2 & 0 & -h_b/4 \\ 0 & 1 & 0 & h_b/2 & 0 & 0 & 0 \\ 0 & 0 & 1 & 0 & 0 & 0 & 0 \\ 0 & 0 & 0 & 1 & 0 & 0 & 0 \\ 0 & 0 & 0 & 0 & 1 & 0 & -1/2 \\ 0 & 0 & 0 & 0 & 0 & 1 & 0 \end{bmatrix} \begin{Bmatrix} \Delta\bar{u}_o \\ \Delta\bar{v}_o \\ \Delta\bar{w}_o \\ \Delta\bar{\theta}_{ox} \\ \Delta\bar{\theta}_{oy} \\ \Delta\bar{\theta}_{zo} \\ \Delta\gamma \end{Bmatrix} \\ &= [T_c]\{\Delta\bar{d}_o\} \end{aligned} \tag{18a}$$

b. Panel zone center to left beam relation:

$$\begin{aligned} \{\Delta\bar{d}_b\} &= \{\Delta\bar{u}_b, \Delta\bar{v}_b, \Delta\bar{w}_b, \Delta\bar{\theta}_{bx}, \Delta\bar{\theta}_{by}, \Delta\bar{\theta}_{bz}\}^T \\ &= \begin{bmatrix} 1 & 0 & 0 & 0 & 0 & 0 & 0 \\ 0 & 1 & 0 & 0 & 0 & h_c/2 & 0 \\ 0 & 0 & 1 & 0 & -h_c/2 & 0 & h_c/4 \\ 0 & 0 & 0 & 1 & 0 & 0 & 0 \\ 0 & 0 & 0 & 0 & 1 & 0 & 1/2 \\ 0 & 0 & 0 & 0 & 0 & 1 & 0 \end{bmatrix} \begin{Bmatrix} \Delta\bar{u}_o \\ \Delta\bar{v}_o \\ \Delta\bar{w}_o \\ \Delta\bar{\theta}_{ox} \\ \Delta\bar{\theta}_{oy} \\ \Delta\bar{\theta}_{oz} \\ \Delta\gamma \end{Bmatrix} \\ &= [T_{bl}]\{\Delta\bar{d}_o\} \end{aligned} \tag{18b}$$

c. Panel zone center to right beam relation:

$$\{\Delta\bar{d}_b\}=\{\Delta\bar{u}_b,\Delta\bar{v}_b,\Delta\bar{w}_b,\Delta\bar{\theta}_{bx},\Delta\bar{\theta}_{by},\Delta\bar{\theta}_{bz}\}^T$$

$$=\begin{bmatrix}1&0&0&0&0&0&0\\0&1&0&0&0&-h_c/2&0\\0&0&1&0&h_c/2&0&-h_c/4\\0&0&0&1&0&0&0\\0&0&0&0&1&0&1/2\\0&0&0&0&0&1&0\end{bmatrix}\begin{Bmatrix}\Delta\bar{u}_o\\\Delta\bar{v}_o\\\Delta\bar{w}_o\\\Delta\bar{\theta}_{ox}\\\Delta\bar{\theta}_{oy}\\\Delta\bar{\theta}_{oz}\\\Delta\gamma\end{Bmatrix}$$

$$=[T_{br}]\{\Delta\bar{d}_o\} \tag{18c}$$

where $\{\Delta\bar{d}_o\}$ are the incremental displacements of panel zone center; $\{\Delta\bar{d}_c\}$ and $\{\Delta\bar{d}_b\}$ are the incremental displacements of the column end and beam end, respectively; h_c and h_b are the depths of cross sections of the column and beam.

(2) Transformation of coordinates

Similar to those discussed in Ref. 11), transformation relations of displacements between the co-rotational coordinate system $(\bar{x}, \bar{y}, \bar{z})$ and the member coordinate system (x, y, z) are derived for the panel zone element. Here, $\{\bar{i}\}=\{\bar{i}_x,\bar{i}_y,\bar{i}_z\}^T$ and $\{g\}=\{g_x,g_y,g_z\}^T$ are used to express the base vectors of the co-rotational coordinates and the member coordinates, respectively; $\{\hat{i}_c\}=\{\hat{i}_{cx},\hat{i}_{cy},\hat{i}_{cz}\}^T$ and $\{\hat{i}_b\}=\{\hat{i}_{bx},\hat{i}_{by},\hat{i}_{bz}\}^T$ are defined as base vectors of cross sections c and b, respectively.

For simplicity of notations, $\{\Delta\bar{\theta}_o\}=\{\Delta\bar{\theta}_{ox},\Delta\bar{\theta}_{oy},\Delta\bar{\theta}_{oz}\}^T$, $\{\Delta\bar{\theta}_c\}=\{\Delta\bar{\theta}_{cx},\Delta\bar{\theta}_{cy},\Delta\bar{\theta}_{cz}\}^T$ and $\{\Delta\bar{\theta}_b\}=\{\Delta\bar{\theta}_{bx},\Delta\bar{\theta}_{by},\Delta\bar{\theta}_{bz}\}^T$ are used to express the incremental rotational components of the center of the panel zone, the connected column end and beam end, respectively, defined in terms of the co-rotational coordinates. Similarly, $\{\Delta\theta_o\}=\{\Delta\theta_{ox},\Delta\theta_{oy},\Delta\theta_{oz}\}^T$, $\{\Delta\theta_c\}=\{\Delta\theta_{cx},\Delta\theta_{cy},\Delta\theta_{cz}\}^T$ and $\{\Delta\theta_b\}=\{\Delta\theta_{bx},\Delta\theta_{by},\Delta\theta_{bz}\}^T$ are the incremental rotational components defined in terms of the member coordinates. The translational components are also expressed as $\{\Delta\bar{u}_{do}\}=\{\Delta\bar{u}_o,\Delta\bar{v}_o,\Delta\bar{w}_o\}$, $\{\Delta\bar{u}_{dc}\}=\{\Delta\bar{u}_c,\Delta\bar{v}_c,\Delta\bar{w}_c\}$ and $\{\Delta\bar{u}_{db}\}=\{\Delta\bar{u}_b,\Delta\bar{v}_b,\Delta\bar{w}_b\}$ in terms of the co-rotational coordinates; $\{\Delta u_{do}\}=\{\Delta u_o,\Delta v_o,\Delta w_o\}$, $\{\Delta u_{dc}\}=\{\Delta u_c,\Delta v_c,\Delta w_c\}$ and $\{\Delta u_{db}\}=\{\Delta u_b,\Delta v_b,\Delta w_b\}$ in terms of the member coordinates.

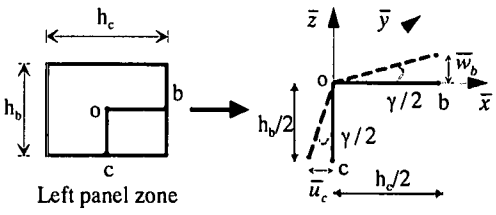

Fig.4 Shear modeling of panel zone in co-rotational coordinate system

For the left panel zone, the displacements due to shear deformation are shown in **Fig.4**. Here, the origin of the co-rotational coordinates is taken at the center of panel zone. The directions of the coordinates are determined such that they coincide with the averaged rotations of nodes c and b expressed by the Euler angles (ϕ_c,θ_c,ψ_c) and (ϕ_b,θ_b,ψ_b). The relations between the co-rotational coordinate system and the member coordinate system are expressed as

$$\{\hat{i}_c\}=[R_c]\{g\};\ \{\hat{i}_b\}=[R_b]\{g\};\ \{\bar{i}\}=[R_G]\{g\} \tag{19a~c}$$

by assuming that the shear deformation of panel zone is relatively small. The relations of rotational components between the two coordinate systems are expressed as

$$\begin{aligned}\{\Delta\bar{\theta}_c\}&=[R_G]\{\Delta\theta_c\};\\ \{\Delta\bar{\theta}_b\}&=[R_G]\{\Delta\theta_b\};\\ \{\Delta\bar{\theta}_o\}&=[R_G]\{\Delta\theta_o\}\end{aligned} \tag{20a~c}$$

$\{\theta_c\}$ and $\{\Delta\theta_b\}$ are expressed by the Euler angles as

$$\{\Delta\theta_c\}=[R_c]^T[BR(\theta_c,\phi_c)]\{\Delta\phi_c,\Delta\theta_c,\Delta\psi_c\}^T;$$
$$\{\Delta\theta_b\}=[R_b]^T[BR(\theta_b,\phi_b)]\{\Delta\phi_b,\Delta\theta_b,\Delta\psi_b\}^T \tag{21a, b}$$

where $[BR(\theta,\phi)]$ is a transient matrix [12]. From Eqs.(18), (20) and (21), we have

$$\{\Delta\bar{\theta}_o\}=\{\Delta\bar{\theta}_c\}+\{0,1/2,0\}^T\Delta\gamma=[R_G]\{\Delta\theta_c\}+\{T_1\}\Delta\gamma$$
$$\{\Delta\bar{\theta}_o\}=\{\Delta\bar{\theta}_b\}-\{0,1/2,0\}^T\Delta\gamma=[R_G]\{\Delta\theta_b\}-\{T_1\}\Delta\gamma \tag{22a, b}$$

and

$$\{\Delta\theta_o\} = \{\Delta\theta_c\} + [R_G]^T \{T_1\}\Delta\gamma \; ; \quad \{\Delta\theta_o\} = \{\Delta\theta_b\} - [R_G]^T \{T_1\}\Delta\gamma \tag{23a, b}$$

Furthermore, from Eqs.(18), the translational displacements due to the panel zone shear deformation are expressed as

$$\{\Delta\bar{u}_{dc}\} = -[h_b/4,\ 0,\ 0]^T \Delta\gamma = -\{T_{c2}\}\Delta\gamma; \quad \{\Delta\bar{u}_{db}\} = [0,\ 0,\ h_c/4]^T \Delta\gamma = \{T_{b2}\}\Delta\gamma \tag{24a, b}$$

On the other hand, the relations of the translational displacements between the two coordinate systems can also be expressed as follows:

$$\begin{Bmatrix} \bar{u}_c \\ \bar{v}_c \\ \bar{w}_c - h_b/2 \end{Bmatrix} = [R_G] \begin{Bmatrix} u_c - u_o \\ v_c - v_o \\ w_c - w_o - h_b/2 \end{Bmatrix} \tag{25a}$$

$$\begin{Bmatrix} \bar{u}_b + h_c/2 \\ \bar{v}_b \\ \bar{w}_b \end{Bmatrix} = [R_G] \begin{Bmatrix} u_b - u_o + h_c/2 \\ v_b - v_o \\ w_b - w_o \end{Bmatrix} \tag{25b}$$

Thus, by taking the increment of Eqs.(25) and using Eqs.(24), the relations of the translational displacements in terms of the member coordinate system are obtained as

$$\{\Delta u_{dc}\} = \{\Delta u_{do}\} - [R_G]^T [CTa]\{\Delta\theta_o\} - [R_G]^T (\{CTb\} - \{T_{c2}\})\Delta\gamma$$
$$\{\Delta u_{db}\} = \{\Delta u_{do}\} - [R_G]^T [BTa]\{\Delta\theta_o\} - [R_G]^T (\{BTb\} + \{T_{b2}\})\Delta\gamma \tag{26a, b}$$

where $[CTa]$, $\{CTb\}$, $[BTa]$, $\{BTb\}$ are transient matrices. Eqs.(23) and (26) give the total displacement relations in terms of the member coordinate system as

$$\{\Delta d_c\} = [RT_c]\{\Delta d_o\} \; ; \quad \{\Delta d_b\} = [RT_b]\{\Delta d_o\} \tag{27a,b}$$

where $[RT_c]_{12\times13}$, $[RT_b]_{12\times13}$ are transformation matrices of the column and the beam, respectively. Similarly, the transformation relations can be obtained for the right panel zone.

In order to ensure the compatibility of deformations at the interfaces between the panel and the beam and column ends during the direct stiffness assembly procedure, the element stiffness matrix of the beam or column connecting to panel zone, are also transformed as

$$[\Delta k_{oc(b)}] = [RT_{c(b)}]^T [\Delta k_{c(b)}][RT_{c(b)}] \tag{28}$$

The incremental panel moment defined as the moment acting on a joint panel is written as

$$\Delta M_p = \Delta k_p \, \Delta\gamma \tag{29}$$

where $\Delta k_p = 2h_c h_b t G_t$ is shear stiffness of the panel zone; t and G_t are thickness and tangent shear modulus of the panel zone.

4. NUMERICAL EXAMPLES

(1) Seismic analysis of single post-type piers

Analytical models used in the present analysis are shown in **Fig.5**, where W=mg is the weight of the pier including the dead load from the superstructure. The dimensions of these models are summarized in **Table 1**. Two models, Pier A and Pier B, with different column slenderness ratios are selected. Pier A has a height of H=7740 mm and constant cross section, while Pier B has a total height of H=15645 mm and stepped cross sections. Considering Bauschinger effect of steel under cyclic loading, the kinematic strain-hardening model with a constant hardening modulus is employed. Thirty elements with a lumped mass are used to discretize both Pier A and Pier B. The number of elements is determined by considering the convergence of solutions. The cross section is divided into 40 elementary areas in order to consider the plastification.

In the present calculation, the seismic behavior of the realistic three-dimensional modeling of bridge piers is compared with that obtained by the conventional in-plane modeling. The in-plane seismic behavior of the bridge piers is calculated under X-directional (weak axis) acceleration component combined with or without Z-direction (U-D) component, whereas the three-dimensional behavior is calculated under both X and Y-directional acceleration components combined with or without Z-direction component. This implies that the seismic loading conditions for each pier consist of four types. In order to consider the dead load of the superstructures, the dead load W=mg is first applied and then the dynamic seismic response analysis is carried out with the dead load kept constant.

Two sets of ground accelerations recorded in the Kobe earthquake are considered as seismic loads. One is the acceleration recorded at the Japan Meteorological Agency (JMA). The other is the acceleration recorded at Japanese Railway Takatori Station (JRT). In order to ensure the maximum peak

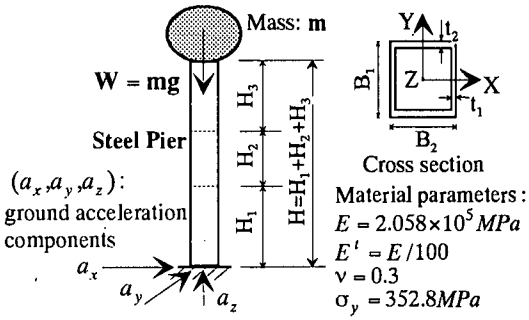

Fig.5 Analytical models for single-post type piers

Table 1 Dimensions of piers

		Pier A	Pier B
m		2,013,000	1,489,000
B1		3100	2500
B2		3000	2500
H1		7740	5000
t1 , t2		30.5, 30.5	34.6, 57.6
H2		———	2200
t1 , t2		———	27.3, 37.1
H3		———	8445
t1 , t2		———	22.8, 26.6
Elastic Natural Period	X	0.369	1.050
	Y	0.361	0.963
	Z	0.090	0.198

unit: kg, mm, sec.

values of ground acceleration along X-direction to be greatest for both JMA and JRT, N-S, E-W and U-D components of JMA are defined as the X, Y and Z components, while E-W and N-S components of JRT are defined as the X and Y components, respectively. The period of the earthquake waves considered for the present calculation is 30 seconds which include the maximum peak values. The time interval adopted in the numerical integration is 0.01sec. for Pier B and Frames A, B; 0.002sec. for Pier A (See Appendix).

As a result of the numerical analysis, sway response displacement histories of pier A subjected to JMA and JRT are shown in **Figs.6** and **7** for the X-directional component. The X-directional maximum sway response displacement and residual displacement of both pier A and B calculated with the respective combinations of the acceleration components are shown in **Table 2**. In **Table 2**, the values of the displacements are normalized by the height H of the piers. Here, the residual deformation, which reflects plastic deformation of piers, is defined as a distance from the center of oscillation to the original equilibrium position when the response of the pier reaches a steady state, as show in **Fig.6**.

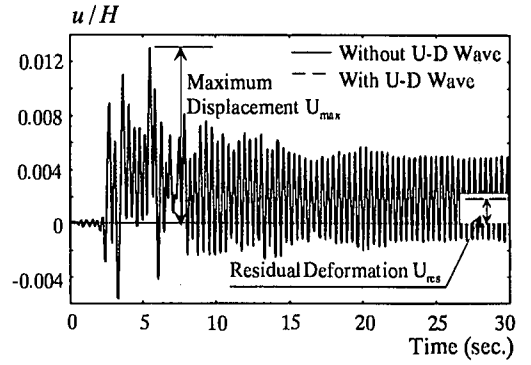

Fig.6 Response displacement of Pier A under in-plane loading (JMA)

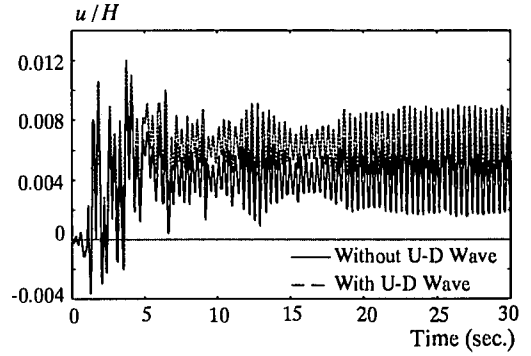

Fig.7 Response displacement of Pier A under in-plane loading (JRT)

First, we discuss the effect of U-D acceleration component based on **Table 3**, where the ratios of the maximum and residual displacements obtained with U-D wave to those without U-D wave are summarized from **Table 2**. The effect on the maximum response displacement is small regardless of the types of bridge piers and the difference of the input accelerograms. The difference of the maximum displacements caused by the vertical acceleration component is less than 14% when N-S and /or E-W acceleration components are considered. In contrast, the residual displacement is much influenced by the vertical acceleration. Especially, the increase of residual displacement caused by the vertical acceleration amounts to 47% for Pier A subjected to X-component wave of JRT. The tendency of the effect induced by the vertical acceleration is, however, not definite. The vertical acceleration component can either increase or decrease the maximum sway response displacement and the residual displacement. This is probably

Table 2 Maximum displacements u_{max}/H and residual displacements u_{res}/H of Pier A and Pier B under different combinations of earthquake waves

Earthquake Waves		U-D Wave	In-Plane (without Y-wave)		3-D (with Y-wave)	
			$u_{max,2D}/H$	$u_{res,2D}/H$	$u_{max,3D}/H$	$u_{res,3D}/H$
JMA	Pier A	×	0.01298	0.00186	0.01580	0.00210
		○	0.01305	0.00174	0.01566	0.00216
	Pier B	×	0.02169	0.00634	0.01534	0.00607
		○	0.02005	0.00436	0.01428	0.00435
JRT	Pier A	×	0.01056	0.00430	0.00997	0.00433
		○	0.01203	0.00630	0.01026	0.00467
	Pier B	×	0.03098	0.01097	0.03169	0.02048
		○	0.03152	0.01340	0.03214	0.02225

Remarks: ○ (×)= U-D wave is (not) considered; (subscripts) 2D=in-plane; 3D=three-dimensional

Table 3 Effect of U-D component on maximum and residual displacements

	Earthquake Wave	$\bar{u}_{max}$ $\bar{u}_{res}$	In-Plane	3-D		Earthquake Wave	$\bar{u}_{max}$ $\bar{u}_{res}$	In-Plane	3-D
Pier A	JMA	$\bar{u}_{max}$	1.01	0.99	Pier B	JMA	$\bar{u}_{max}$	0.92	0.93
		$\bar{u}_{res}$	0.94	1.03			$\bar{u}_{res}$	0.69	0.72
	JRT	$\bar{u}_{max}$	1.14	1.03		JRT	$\bar{u}_{max}$	1.02	1.01
		$\bar{u}_{res}$	1.47	1.08			$\bar{u}_{res}$	1.22	1.09

Remarks: $\bar{u}_{max} = u_{max,with\ U-D}/u_{max,without\ U-D}$, $\bar{u}_{res} = u_{res,with\ U-D}/u_{res,without\ U-D}$

Table 4 Effect of coupling of horizontal waves on maximum and residual displacements

	Earthquake Wave	U-D Wave	$\frac{u_{max,3D}}{u_{max,2D}}$	$\frac{u_{res,3D}}{u_{res,2D}}$		Earthquake Wave	U-D Wave	$\frac{u_{max,3D}}{u_{max,2D}}$	$\frac{u_{res,3D}}{u_{res,2D}}$
Pier A	JMA	×	1.22	1.13	Pier B	JMA	×	0.71	1.04
		○	1.20	1.24			○	0.71	1.00
	JRT	×	0.94	1.01		JRT	×	1.02	1.87
		○	0.85	0.74			○	1.02	1.66

because at some special point of time, such as, the point at which the sway displacement reaches its maximum value, the vertical acceleration does not necessarily produce a compressive inertia force that leads to the increase of the sway displacement by $P-\Delta$ effect. The up-ward inertia force results in a tensile force that leads to the decrease of the sway displacement.

Next, we examine the coupling effect of N-S and E-W acceleration components on the seismic behavior of the piers based on **Table 4**, where the ratios of the maximum and residual displacements obtained with both X- and Y-wave to those without Y-wave are summarized from **Table 2**. The consideration on Y acceleration component in addition to X-component can either increase or decrease the maximum response displacement and the residual displacement. The maximum increase caused by Y-component is 22% for the maximum response displacement and 87% for the residual displacement. This implies that the customary in-plane modeling of bridge piers may sometimes underestimate the effect of the seismic waves on their ultimate behavior. From these results, it can be said that the coupling effect of the horizontal acceleration components is more significant than that of the vertical acceleration component.

(2) Seismic analysis of portal frame

Portal frame-type bridge pier models presented by Miki et al [11] are used in our analysis. The details of these models are shown in **Fig.8**. The dimensions and material properties are summarized in **Table 5**. Frame B has the same material properties and dimensions as Frame A except for the beam section (Sec.4). As a constitutive law, the kinematic hardening model with a constant hardening modulus is used for beams, columns and panel zones. After yielding, $E' = 0.05E$ is assumed for panel zones

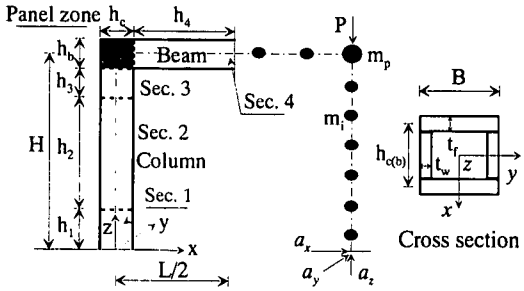

Fig.8 Portal frame type models

Table 5 Dimensions of frames

Frame A (Frame B)				
Sec. i	h_i (mm)	t_{fi} (mm)	t_{wi} (mm)	σ_y (MPa)
1	3,744	32.0	25.6	383
2	10,051	26.0	20.8	281
3	605	36.0	28.8	270
4	11,520	36.0 (30.0)	28.8 (20.0)	270 (235.2)
H=15.0m, L=24.0m, h_c=0.96m, h_b=1.2m, B=1.2m, m_p=3.168×10^{5}kg, T_{Ax}=1.12s; T_{Bx}=1.012s				

Remarks: data in parenthesis are for Frame B; m_p=concentrated mass located at the center of panel zone; mass density of steel $\rho = 7.85\times10^3 kg/m^3$; T_{Ax}, T_{Bx} : the natural periods of Frame A and B along X-direction; panel zone web thickness t_{wp}=28.8mm.

(Kato et al [5]), while $E' = 0.01E$ is adopted for columns and beams. Lumped masses are considered for the respective nodes of beam, column and panel zone elements. The seismic waves used in the present analysis are those of JMA and JRT as described in **Section. 4 (1)**. In case of the in-plane loading, only X-component of the seismic waves is applied, whereas all the three components are applied in the three-dimensional loading.

Sixty elements are used to discretize both Frame A and B; that is, twenty-five elements for each column and ten elements for the beam. The cross section are divided into 40 elementary areas in order to consider the plastification.

First, the difference between the present shear panel zone modeling (P-Z model) and conventional centerline-to-centerline modeling (C-C model) with rigid beam-to-column connections is investigated. **Figure.9** shows the response displacement histories of Frame A subjected to JMA and JRT waves. Here, u is the averaged sway displacement at the tops of two columns. As a result of the numerical analysis under in-plane loading (JMA), the averaged horizontal restoring force R_f vs. sway displacement u/H relations for Frames A and B are shown in

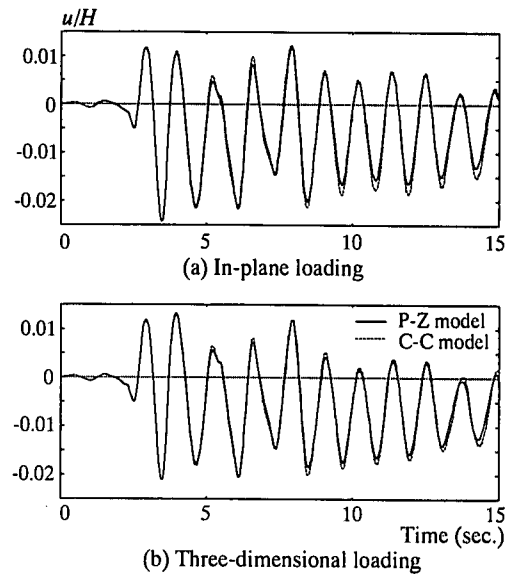

Fig.9 Sway response displacement histories of Frame A subjected to JMA waves

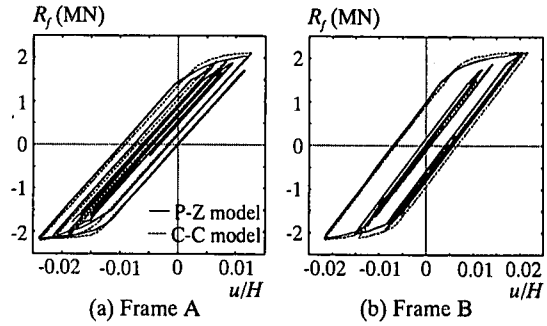

Fig.10 Restoring force vs. sway displacement curves

Fig.10. In order to obtain smooth hysteretic curves, only the concentrated mass m_p at the tops of the columns is considered in calculating R_f vs. u/H relations.

From **Fig.9**, it can be seen that almost the same results are obtained up to the maximum response displacement, regardless of whether the panel zone deformation is considered or not. After the maximum response displacement is experienced, the difference between the two models becomes somewhat noticeable. The restoring force vs. sway displacement curves also show that the C-C modeling gives the same stiffness of the frames as P-Z modeling in the elastic range. This is because the C-C modeling results in greater member lengths than actual ones, which reduces the frame's stiffness and compensates the error [5]. However, in the plastic range, the stiffness and strength of the P-Z models are apparently smaller than those of the C-C models as can be seen from **Fig.10**.

Table 6 Maximum and residual sway displacement U_{max}/H , U_{res}/H (%)

Earthquake waves		Frame A		Frame B	
		U_{max}	U_{res}	U_{max}	U_{res}
JMA	2D	2.43 *1.01	0.51 *0.84	2.25 *1.00	0.04 *3.81
	3D	2.11 *1.00	0.63 *0.95	2.14 *1.00	0.19 *0.98
JRT	2D	3.92 *1.02	1.23 *1.03	2.50 *1.04	0.27 *1.36
	3D	3.60 *0.99	1.37 *0.94	2.86 *1.08	1.22 *1.33

Remarks: 2D, 3D are the same as those defined in **Table 2**; data with * = $u/u_{c\text{-}c}$; $u_{c\text{-}c}$: obtained by the C-C modeling.

Finally, the seismic behavior of frames is discussed in terms of the difference caused by the loading patterns; that is, in-plane loading and three-dimensional loading. In addition to the maximum sway displacements and residual displacements summarized in **Table 6**, we show the sway response displacement histories and cumulative plastic strain histories in **Figs.11**, **12** and **13**. In **Fig.12**, the cumulative plastic strains are shown for three sections of columns as defined in **Fig.8**. In this case, the cumulative plastic strain $\varepsilon_{ep}\,(or\ \gamma_{ep})$ is the averaged plastic strain for the respective sections and is defined as $\varepsilon_{ep}\,(or\ \gamma_{ep}) = (\int \bar{\varepsilon}^{p} dA)/A$, where $\bar{\varepsilon}^{p}$ is the equivalent plastic strain; A is the cross-sectional area. The panel zone cumulative plastic strain shown in **Fig. 13** is averaged over the two panel zones for each frame .

It can be seen from **Table 6** and **Fig.11** that although the coupling of earthquake waves produced uncertain tendency for the maximum response displacements of frames, the residual deformations induced by the coupling are larger than those by in-plane loading. Since the magnitude of the residual displacement is influenced by the plastification of frames, we examine some details of the plastification patterns based on **Figs.12** and **13**. From these figures, it is observed that the plastification pattern is much influenced by the loading patterns. That is, the in-plane loading results in more plastification in the panel zone whilst the three-dimensional loading causes more plastification in columns. These results are consistent with the experimental results obtained by Miki and Kotoguchi[10]. The increased plastification in columns leads to a larger residual sway displacement. This phenomenon shows that there exits different failure mechanism according to whether piers are subjected to in-plane loading or three-dimensional loading.

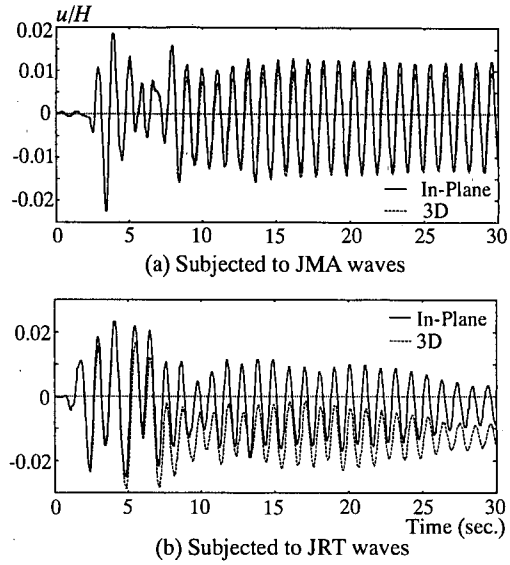

Fig.11 Sway response displacement histories of Frame B

5. SUMMARY AND CONCLUDING REMARKS

In this paper, a three-dimensional numerical analysis method of space frames was presented. In this method, both geometric and material nonlinearity were included. Furthermore, a joint element was introduced to consider the shear deformation along with the rigid body motion of beam-to-column panel zones. With this method the seismic behaviors of single post-type and portal frame-type steel bridge piers subjected to either in-plane or three-dimensional ground motions were investigated. The results obtained from the present research are summarized in the following.

(1) The residual deformation of the single post-type piers is somewhat affected by the vertical acceleration component, whilst the maximum displacement is less affected.

(2) The coupling of the two horizontal acceleration components affects both the maximum response displacement and the residual displacement. Therefore, it can be concluded that the in-plane modeling of single post-type piers may result in an inaccurate prediction for both the maximum response displacement and the residual displacement.

(3) For portal frame-type piers, the conventional centerline-to-centerline modeling may overestimate the stiffness and strength of frames when the structures reach elasto-plastic region.

(4) The plastification pattern of portal frame-type

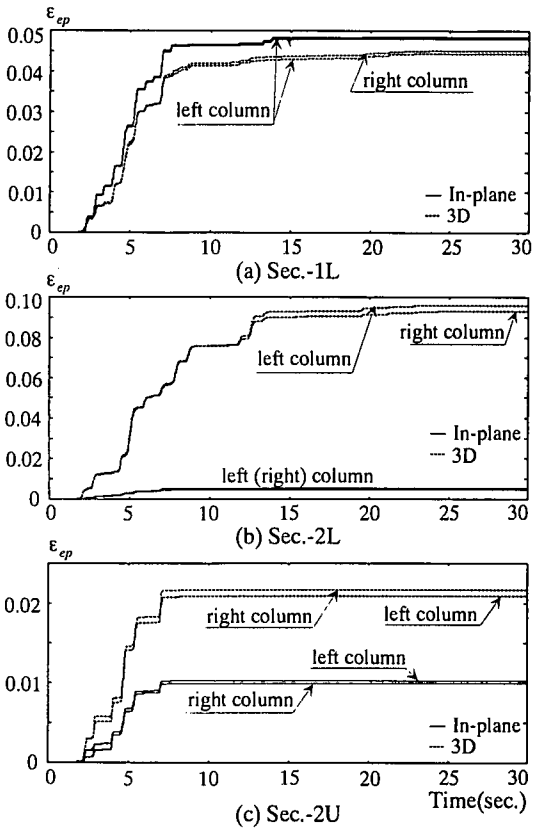

Fig.12 Time histories of cumulative plastic strain in cross sections of Frame B (JRT)

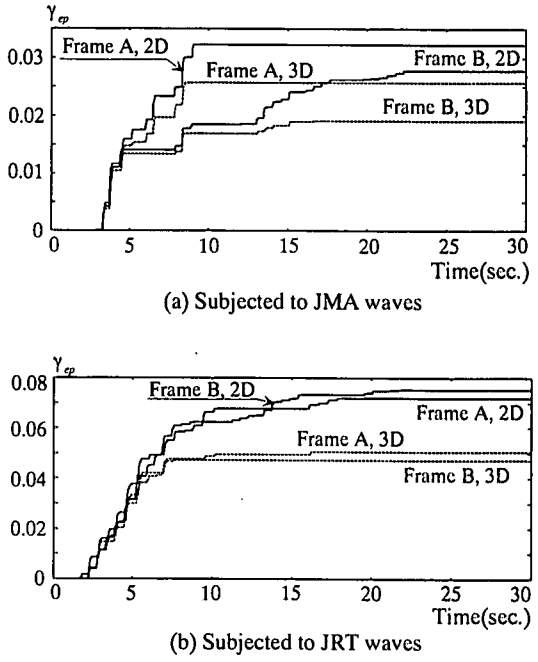

Fig.13 Time histories of cumulative plastic strain in panel zone

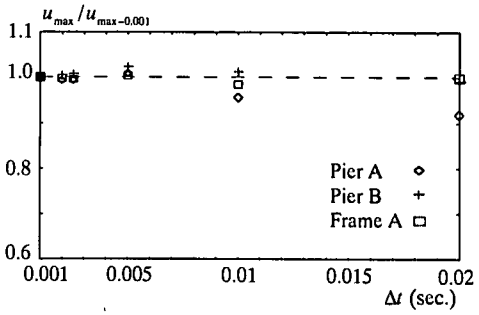

Fig.A Convergence of solutions due to time intervals

bridge piers is much influenced by the loading patterns. That is, the in-plane loading results in more plastification in the panel zone whilst the three-dimensional loading causes more plastification in columns. The increased plastification in columns leads to a larger residual sway displacement.

APPENDIX

In order to determine a suitable time interval Δt for the numerical integration, the convergence of numerical solutions is examined for Piers A , B and Frame A with using different time intervals. For simplicity, the convergence of solutions is not examined for Frame B, since this frame has the same dimensions as frame A except for its beam. In **Fig.A**, the maximum sway response displacement u_{max} vs. time interval Δt is shown for these structures. As seismic loads, N-S and U-D components of JMA are applied to the X- and Z-directions of Piers A and B, while N-S, E-W and U-D components of JMA are applied to the X-, Y- and Z-directions of Frame A. The time intervals examined here are 0.001, 0.002, 0.0025, 0.005, 0.01 and 0.02 sec.. In **Fig.A**, the maximum sway response displacement u_{max} is normalized by the maximum response displacement $u_{max-0.001}$ when Δt is 0.001 sec.. From **Fig.A**, it can be seen that all time intervals yields virtually the same solutions for Pier B and Frame A. However, for Pier A, the difference of solutions becomes larger than 4.5% when Δt exceeds 0.01 sec. For this reason and considering the computational efficiency, the time interval 0.01sec is chosen for Pier B and Frames A, B and 0.002sec for Pier A.

REFERENCES

1) Krawinkler, H., Bertero, V.V. and Popov, E.P. : Shear

Behavior of Steel Frame Joints. *J. Struct. Divi.* ASCE. Vol.101, No. ST11, pp.2317-2336, 1975.
2) Krawinkler, H. and Popov, E.P. : Seismic Behavior of Moment Connections and Joints *J. Struct. Divi.* ASCE. Vol.108, No. ST2, pp.373-391, 1982.
3) Ghobarah, A., Korol, R.M. and Osman, A. : Cyclic Behavior of Extended End-Plate Joints. *J. Struct. Engrg.* , ASCE, Vol.118, No.5, pp.1333-1353, 1992.
4) Kato, B. : Beam-to-Column Connection Research in Japan. *J. Struct. Divi.* ASCE. Vol.108, No. ST2, pp.343-360, 1982.
5) Kato, B., Chen, W.F. and Nakao, M. : Effects of Joint-panel Shear Deformation on Frames. *J. Constr. Steel Res.*, **10**, pp.269-320, 1988.
6) Lui, E.M. and Chen, W.F. : Frame Analysis with Panel Zone Deformation. *Int. J. Solids and Struct.*, Vol.22, No.12, pp.1599-1627, 1986.
7) Liew, J.Y.R. and Chen, W.F. : Analysis and Design of Steel Frames Considering Panel Joint Deformations. *J. Struct. Engrg.* , ASCE, Vol.121. No.10, pp.1531-1540, 1995.
8) Leger, P. , Paultre, P. and Nuggihalli, R. : Elastic Analysis of Frames Considering Panel Zones Deformations. *Comput. & Struct.*, Vol.39, No.6, pp.689-697, 1991.
9) Tsai, K.C. and Popov, P. : Seismic Panel Zone Design Effect on Elastic Story Drift in Steel Frames. *J. Struct. Engrg.* , ASCE, Vol.116, No.12, pp.3285-3301, 1990.
10) Miki, T.. and Kotoguchi, H. : Experimental Studies of Collapse Behaviors and Deformation Capacity of Steel Beam-to-Column Connections. *J. Struct. Engrg*, JSCE, Vol.37A, pp.121-134, 1991 (in Japanese).
11) Miki, T., Kotoguchi, H. and Osada, Y. : Inelastic Earthquake Response and Collapse Modes of Steel Portal Frames with Variable Cross-Section. *J. Struct. Engrg.*, JSCE, Vol.43A, pp.205-216, 1997 (in Japanese).
12) Goto, Y., Li, X.S., Kasugai, T. and Obata, M. : Analysis of Greenhill Problem by a Co-Rotational Method. *J. Struct. Engrg*, JSCE, Vol.41A, pp.411-420, 1995.
13) Simo, J.C. and Vu-Quoc, L. : A Three-Dimensional Finite Strain Rod Model--Part Ⅱ : Computational Aspects. *Comput. Meths. Appl. Mech. Engrg.*, **58**, pp.79-116, 1986.
14) Simo, J.C. and Taylor, R.L. : A Return Mapping Algorithm for Plane Stress Elastoplasticity. *Int. J. Numer. Methods Engrg.*, Vol.22, pp.649-670, 1986.
15) Dodds, R.H. : Numerical Techniques for Plasticity Computations in Finite Element Analysis. *Comput. & Struct.*, Vol.26, No.5, pp.767-779, 1987.
16) Crisfield, M.A. : *Non-linear Finite Element Analysis of Solids and Structures. Volume 1: Essentials.* John Wiley & Sons, 1991.
17) Hinton, E. and Owen, D.R.J. : *An Introduction to Finite Element Computations*. Pineridge Press, Swansea, UK., 1979.
18) Nishino, F. and Hasegawa, A. : Thin-Walled Elastic Members. *J. Faculty of Engrg.*, The University of Tokyo (B), Vol.XXXV, No.2, pp.109-190, 1979.
19) Owen, D.R.J. and Hinton, E. : *Finite Element in Plasticity (Theory and practice).*, Pineridge Press Limited, Swansea, U.K. pp.141-144, 1980.
20) El-Khenfas, M.A. and Nethercot, D..A. : Ultimate Strength Analysis of Steel Beam-Columns Subject to Biaxial Bending and Torsion. *Res Mechanica.* **28**, pp.307-360, 1989.
21) Bathe, K.J., Ramm, E. and Wilson, E.L. : Finite Element Formulations for Large Deformation Dynamic Analysis. *Int. J. Numer. Methods Engrg.*, Vol.9, pp.335-386, 1975.

(Received September 26, 1997)

隅角部の変形を考慮した骨組の三次元非線形地震応答解析に関する研究

り　暁松・後藤　芳顯

隅角部のせん断変形を考慮した，骨組の三次元複合非線形地震応答解析法を提示した．ここで，幾何学非線形性は剛体変位除去の手法により厳密に考慮し，材料非線形性はJ2流れ則の範囲で混合硬化則に基づく．また，ねじりによるせん断の他に，細長比の小さな鋼製橋脚を対象とするため，曲げせん断変形も考慮している．鋼製橋脚の地震時終局挙動の解析例から，三次元解析と二次元解析とではかなり差が生じ，二次元解析による設計が危険側になる場合もあること，さらに，三次元解析では，塑性化が隅角部に比べ，柱により生じやすい傾向にあることなどが判明した．